Crystallinity of Silicon-Shells Deposited onto Germanium and Silicon Nanowires for Core-Shell Nanostructures and Nanotubes

Ardeshir Moeinian, Nicolas Hibst, Dorin Geiger, Johannes Biskupek, and Steffen Strehle

***Abstract*—Core-shell nanowires are an essential component of numerous nanoscale device concepts. In this study, germanium and silicon nanowires were synthesized bottom-up using the vapor-liquid-solid technique and successively modified with a silicon shell. The shell synthesis was studied with focus to the crystallinity but includes as well the electrical characteristics of n- and p-doped radial core-shell nanowire devices. Furthermore, the influence of certain post-annealing procedures on the crystallinity of the core-shell nanowires are discussed. We demonstrate that the crystallinity of the silicon shell can be tuned from single-crystalline to amorphous in a controlled manner, independent on a p- or n-type doping, by deliberate adjustment of the growth parameters.**

***Index Terms*—Characterization, nanotubes, nanowires, raman scattering, transmission electron microscopy.**

I. Introduction

THE bottom-up synthesis of radial core-shell nanowires supports the direct fabrication of complex nanowire devices with adjustable dimensions and with control over the spatial doping levels that can hardly be achieved by conventional top-down microfabrication techniques. An important example is the fabrication of radial homo- and hetero-structures as well as pn-junctions, here with emphasis to the semiconductor materials germanium and silicon [1], [2]. The implementation of such structures or junctions in several nanoscale devices such as sensors, transistors, electronic switches, battery anodes as well as solar cells, is under discussion for some time [3], [4]. State-of-the-art device fabrication relies on selective shell etchings as well as on deliberately adjusted optical and electrical characteristics, which are directly related to the crystallinity of the shell [5].

Although silicon nanowire (SiNW) and germanium nanowire (GeNW) core-shell structures seem to promise significant qualities and novel applications [6], fundamental studies, including full control over materials electronic properties, dimensions and crystallinity with high reproducibility, are still not sufficient. The aim of this work is to provide insights into the synthesis of germanium-silicon (Ge-Si) and silicon-silicon (Si-Si) core-shell nanowires based on the vapor-liquid-solid (VLS) growth and thermally induced chemical-vapor-deposition (CVD). The influence of post-annealing procedures as well as effects emerging from the nanowire growth conditions are discussed. By exploiting several material characterization and processing methods, crystallinity and electronic properties of the synthesized core-shell nanowires are assessed. Moreover, it is illustrated that the removal of the germanium core, in case of Ge-Si core-shell nanowires, by selective H_2O_2 etching, makes the synthesis of silicon nanotubes possible. Silicon nanotubes can be used for example in combination with suitable microfluidics as ion-sensitive flow-through field-effect-transistors [7]. The results of this study support therefore also intrinsically the overall enhancement of silicon nanotube properties in the direction of further device miniaturization and adjustable microstructural properties based on a reproducible and improved morphology.

Manuscript received November 12, 2016; revised February 21, 2017; accepted March 28, 2017. Date of publication April 7, 2017; date of current version September 6, 2017. This work was supported by the experimental support by S. Jenisch (Institute of Electron Devices and Circuits, Ulm University). The financial support by the German Federal Ministry of Education and Research (BMBF FKZ: 13N12545) is gratefully acknowledged.This work was supported by the Federal Ministry of Research and Education (Germany) – FKZ 13N12545: NanoMatFutur. The review of this paper was arranged by associate editor M. J. Amman. *(Corresponding author: Ardeshir Moeinian.)*

The authors are with Ulm University, 89081 Ulm, Germany (e-mail: ardeshir.moeinian@uni-ulm.de; nicolas.hibst@uni-ulm.de; dorin.geiger@uni-Ulm.de; johannes.biskupek@uni-ulm.de; steffen.strehle@uni-ulm.de).

Digital Object Identifier 10.1109/TNANO.2017.2692099

II. Experimental Procedure

In general, single crystalline GeNWs and SiNWs were synthesized by a gold catalyzed VLS growth with diameters ranging from 20 to 50 nm using gold colloids dispersed on single-crystalline silicon or sapphire substrates. As an initial step, the growth substrate was coated with a layer of poly-l-lysine in order to enhance the adhesion and spatial distribution of the deposited gold colloid particles. VLS nanowire synthesis was carried out in a quartz tube furnace with a gas manifold and a vacuum pump (base pressure 0.08 mbar) connected to the quartz tube. After VLS synthesis, nanowires were overgrown with a silicon shell with a total thickness ranging from 25 to 200 nm utilizing a conventional thermal CVD process.

For Si-Si core-shell nanowires, two different synthesis strategies were employed. At first, SiNWs were grown using a mixture of 100 sccm of 2% silane in helium, 10 sccm hydrogen and 10 sccm of 100 ppm diborane in helium as p-dopant at a temperature of 475 °C and 100 mbar working pressure. Subsequently, the silicon shell was grown onto the nanowires using either of the two strategies explained here. The first strategy represents a single step shell growth at a lower temperature (500–540 °C) and at a chamber pressure of 50 mbar after the removal of the

gold catalyst (labeled single-step). A solution of iodine (5 g) and potassium iodine (22 g) dissolved in water (220 ml) is used as gold catalyst etching agent. Gold catalyst removal prevents axial elongation of the silicon nanowires during shell growth. After the removal of the gold catalyst, a short HF dip is performed in order to remove any oxide layer from the side walls of the silicon nanowires, immediately before the substrate is inserted into the CVD chamber. Silane (2% diluted in helium) flow rate was set at 100 sccm along with a phosphine flux of 10 sccm (200 ppm phosphine diluted in helium) as dopant gas that results in an n-doped shell. Shell growth under these conditions occurs at a velocity of approximately 2.5 nm/min. In the second strategy the growth conditions are altered in a way that shell growth is done with the gold catalyst still intact (labeled double-step). In order to realize this, the gold catalyst must be rapidly encapsulated by silicon to cut off the catalyst from the silane precursor supply, which consequently suppresses the nanowire elongation. An encapsulation of the catalyst is triggered by an increased silane decomposition or deposition rate at the surface as readily obtained at elevated temperatures. Therefore, this step is performed for 2 minutes at a temperature of 650 °C with a 50 sccm flux of 2% silane diluted in helium and a pressure of 33 mbar resulting here in a 15 nm thick Si shell that encapsulated the gold catalyst effectively. The shell thickness can be increased successively also at a lower temperatures, as done here, in the same manner as single-step shell synthesis.

Ge-Si core-shell nanowires with radial heterojunction are synthesized by growing at first a GeNW by gold catalyzed VLS synthesis followed as well by either a single- or a double-step shell growth. The single-step shell growth consists of a rapid overgrowth deposited at 650 °C encapsulating the GeNWs and the gold catalyst. This prevents again axial elongation of nanowires similar to the first part of the Si-Si double step shell growth. This step is done using 65 sccm of silane (2% diluted in helium) and 6 sccm of phosphine (200 ppm diluted in helium) for n-type doping under 20 mbar working pressure. For the double-step shell growth, shell thickness is increased by an additional shell growth step carried out at 500 °C using 100 sccm of silane (2% diluted in helium) and 10 sccm of phosphine (200 ppm diluted in helium) under 50 mbar working pressure. GeNWs were grown using monogermane gas (2% diluted in helium). The growth of GeNWs is initiated by a 300 s growth process at 295 °C and a chamber pressure of 400 mbar. Keeping the same monogermane flow rate, a second step is performed for one hour at 270 °C and 135 mbar for nanowire elongation similar to that reported in [8].

In order to perform electrical and structural characterizations, nanowires were released from the growth substrate and immersed in isopropanol by applying ultra-sonication. This enables the deposition of nanowires out of solution onto grids suitable for transmission electron microscopy (TEM) and onto substrates, which were used for further device fabrication processes. In order to electrically characterize Si-Si core-shell nanowires, selective shell etching is required thus enabling deposition of metal contacts on both core and shell parts of the nanowire. This was done by an etching step in aqueous KOH (30%) for 15 s at 60 °C removing parts of the nanowire not protected by poly(methyl-methacrylate) (PMMA) resist patterned by electron beam lithography. The silicon oxide layer was removed by an HF dip before performing the KOH etch. Prior to deposition of metal contacts and nanowire deposition on TEM grids, a set of samples underwent heat treatment in a rapid thermal annealing furnace with a nitrogen atmosphere at 650 °C for 30 and 300 s. TEM investigations were carried out using a Philips CM 20 electron microscope operating at 200 kV. For Raman measurements, SiNWs were grown on sapphire substrates to prevent any overlap of signals emerging from the substrate with signals from the nanowires. Raman spectroscopy measurements were done using a Coherent Innova 90 Ar+ ion laser, operated at 514 nm.

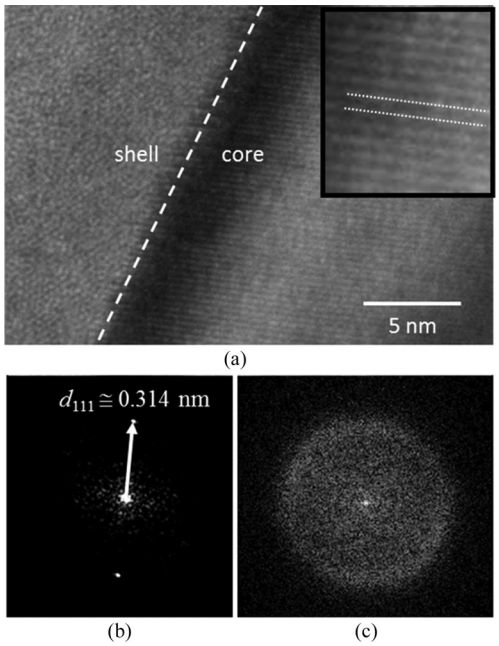

Fig. 1. (a) HRTEM image of a single-step Si-Si core-shell nanowire. The inset in (a) represents a magnified area of the crystalline nanowire core with indicated lattice planes. (b) Diffractogram of the core obtained from a sub-image (after applying Hanning window), which shows the spot pattern of [111] planes of silicon. (c) Diffractogram captured within the shell area indicating an amorphous structure.

III. Results

A. Si-Si Core-Shell Nanowires

SiNWs grown through VLS growth lead to single crystalline nanowires grown in a favored crystalline direction. SiNWs have been observed to grow in different crystalline directions, namely $\langle 111 \rangle$ and $\langle 110 \rangle$, where wires with diameters above 20 nm tend to grow in $\langle 111 \rangle$ direction and wires with smaller diameters than 20 nm grow in $\langle 110 \rangle$ direction [9]. There have been reports of nanowires growing in the unfavorable $\langle 100 \rangle$ direction through guided epitaxial growth on a $\langle 100 \rangle$ substrate [9].

Fig. 1 illustrates a high resolution TEM (HRTEM) image of a single-step Si-Si core-shell nanowire. The shell morphology seems to be almost exclusively amorphous while the core is always, as expected, crystalline. This can be seen in the bright field image Fig. 1(a) as the crystal planes of the nanowire core discontinue at the boundary to the shell region. The

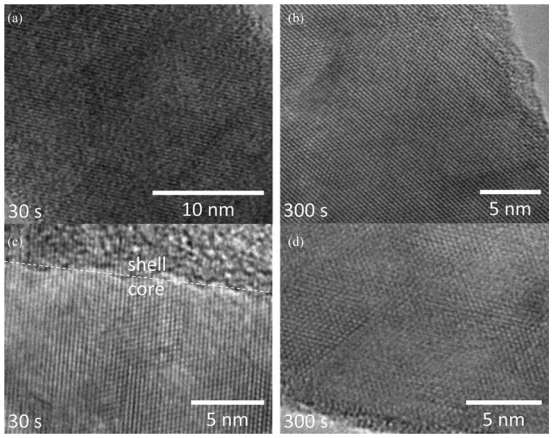

Fig. 2. HRTEM images of single-step Si-Si core-shell nanowires showing the silicon shell morphology after different annealing times. 30 s annealing result in the presence of both, (a) crystalline and (b) amorphous shell structures where the core is still distinguishable. (c) Fully single-crystalline core-shell nanowire with epitaxial interface after 300 s of annealing. (d) 300 s of annealing results in a fully polycrystalline shell structure where no remaining amorphous regions are visible.

inset in Fig. 1(a) shows a magnified area of the core with the crystal planes indicated. The contrast along the diameter of the nanowire stems from changes in thickness due to the cylindrical shape of the nanowire. The crystal plane appear to represent the silicon [111] planes. This can be seen in the diffractogram of the nanowire core given in Fig. 1(b), which shows a spot pattern typically associated with silicon [111] planes. The measurement of the lattice plane distance yields here 0.314 nm. Fig. 1(c) shows the diffractogram of the shell area lacking a distinct spot pattern, which indicates an amorphous structure.

Although as-grown single-step Si-Si core-shell nanowires possess an amorphous shell, the microstructure of the shell region can be successively altered by adequate post-annealing as shown in the HRTEM images in Fig. 2. Fig. 2(a) and (b) are examples of 30 s annealed core-shell nanowires. Thirty seconds annealing at 640 °C results in both, crystalline (a) and amorphous (b) shells. The crystallization process of the shells with respect to the annealing time seems to be dependent on the nanowire diameter. Amorphous shell structures for nanowires with a total diameter of less than 20 nm become completely crystalline within the first 30 s of annealing while for larger diameters amorophous or partly amorphous shell regions persist. Shell structures of nanowires with larger diameters require therefore longer annealing times for the entire shell structure to crystallize. After 300 s of annealing, all shell structures irrespective of the nanowire diameter are crystalline. In some cases the crystal planes of the shells are aligned to that of the nanowire core implying an epitaxial relationship [see Fig. 2(c)] where no distinct core-shell structure can be observed. In case of a polycrystalline shell, a distinct single-crystalline core cannot be detected due to differently oriented crystalline regions in the shell encapculating the core structure as shown in Fig. 2(d).

As shown in the HRTEM images of double-step Si-Si core-shell nanowires provided in Fig. 3(a), the shell exhibits some crystalline areas already in the as-grown state. The initial formation of crystalline regions is due to the first part of shell

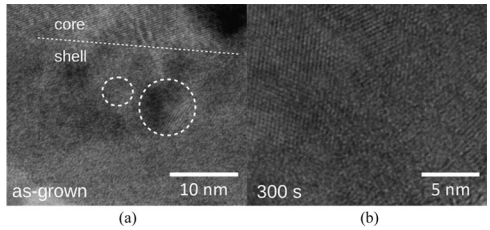

Fig. 3. HRTEM images of double-step Si-Si core-shell nanowires. (a) TEM image of as-grown core-shell nanowires; circles indicate crystalline areas along the shell structure. (b) TEM image of a core-shell nanowire annealed for 300 s indicating a fully polycrystalline structure.

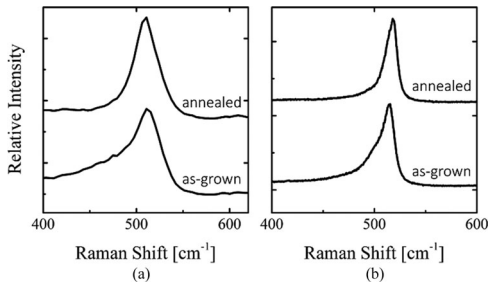

Fig. 4. Raman spectra of (a) single-step and (b) double-step Si-Si core-shell nanowires. Post-annealing results in a lower intensity of the amorphous silicon Raman peak at 495 cm^{-1} for both single- and double-step core-shell nanowires.

growth being carried out at 650 °C. The crystalline regions are embedded into an amorphous matrix. The reason for a lacking single-crystalline shell, which could be potentially expected from the higher synthesis temperature within the first shell growth step, is still under discussion but might be linked to the diffusion of gold from the catalyst along the nanowire backbone or to a reaction with residual oxygen triggered by the higher temperature. In contrast to single-step Si-Si core shell nanowires and based on the initial presence of individual crystals, post-annealing at 640 °C for 300 s results in a fully polycrystalline rather than a single-crystalline shell [see Fig. 3(b)]. The result of a polycrystalline shell is manifested in differently oriented crystalline areas in the shell structure. As before, a distinct single-crystalline nanowire core cannot be clearly detected in Fig. 3(b) due to the overlap with the polycrystalline shell areas encapsulating the nanowire core.

Besides TEM, Raman spectroscopy, as a nondestructive and rapid analytical method was used in this work in order to further analyze the effect of annealing on core-shell microstructure. Fig. 4 illustrates Raman spectra of as-grown and annealed Si-Si core-shell nanowires.

Crystalline silicon (c-Si) exhibits a sharp Raman feature at 520 cm^{-1}. Different Raman features begin to manifest as silicon structure changes from single crystalline to poly- and nanocrystalline [10]. SiNWs have been reported to exhibit peaks at around 150, 300, 520 and 964 cm^{-1} [11]. As observed by [12], with decreasing nanowire diameter these peaks shift to lower frequencies and the full width at half maximum (FWHM) of the peaks increases. The peak occurring at 520 cm^{-1} corresponds to the first order transverse optical mode of c-Si (F_{2g}). A downshift of the c-Si peak and its asymmetric broadening due to quantum

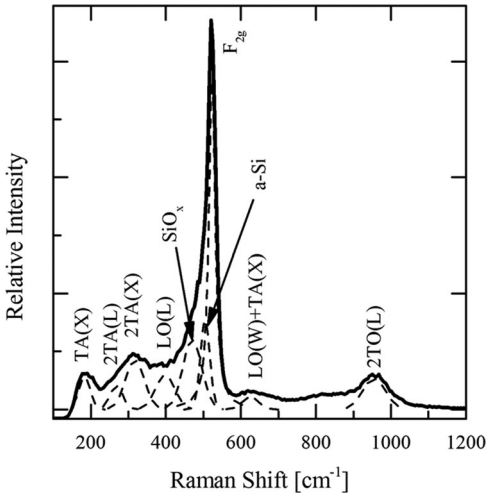

Fig. 5. Peak assignment and peak deconvolution of a Raman spectrum originating from Si-Si core-shell nanowires.

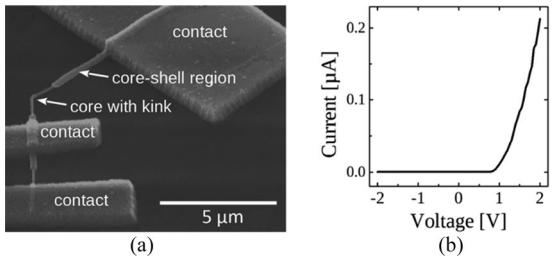

Fig. 6. (a) SEM image of a kinked p-doped core and n-doped shell Si-Si nanowire device. (b) Current-voltage behavior of a core-shell pn-junction with a clear rectifying behavior.

confinement is explained in [13]. Additionally, SiNWs are typically covered by a thin oxide layer, which gives rise to a broad Raman peak at 480 cm^{-1} and has significant effects on the F_{2g} peak causing it to become broader and have a stronger baseline [11], cf. [12]. The peaks centered at 150, 300 and 960 cm^{-1} are assigned to transverse acoustic TA(X), second order transverse acoustic 2TA(L), and second order transverse optical overtones, respectively. A broad peak centered at 495 cm^{-1} is attributed to amorphous silicon (a-Si) [13]. Due to the similarity of Raman features of different SiNW structures, a detailed analysis of peak position and FWHM is required in order to make microstructural analysis possible. The Raman features as shown in Fig. 4 are analyzed using computer-aided deconvolution. Fig. 5 illustrates an example of a Si-Si core-shell Raman spectrum peak analysis and assignment.

Both, single- and double-step as-grown core-shell nanowires manifest similar Raman features and follow the same pattern after annealing. As-grown Raman spectra of both types of Si-Si core-shell nanowires show downshift and asymmetrical broadening of the c-Si peak (F_{2g} peak). The occurrence of a shoulder at 495 cm^{-1} next to c-Si peak of the Raman spectra of as-grown nanowires is due to the presence of amorphous silicon (assigned as a-Si). Deconvolution of the as-grown and annealed Raman spectra of single-step core-shell nanowires [see Fig. 4(a)] reveals that the ratio of a-Si (495 cm^{-1}) to c-Si (F_{2g} peak at around 514 cm^{-1}) intensities (peak height ratio) decreases by about 45 % from 0.2 to 0.11 after annealing. By comparing the F_{2g} Raman peak of as-grown and annealed core-shell nanowires we observe a decrease in FWHM, which is a result of higher crystalline order in annealed samples. As bond disorder increases due to smaller silicon crystallite sizes, $k \sim 0$ selection rule is relaxed and contributions from other phonon lines is superimposed on the c-Si peak causing an increase in its FWHM [10].

Similarly, the Raman spectra of double-step core-shell nanowires [see Fig. 4(b)] reveal that after annealing the ratio of a-Si to c-Si intensities (peak height ratio) decreases by about 40 % from 0.19 to 0.11. Additionally, the Raman peak position of c-Si, which has a large red shift in as-grown double-step core-shell nanowires, shifts from 514 to 518 cm^{-1} closer to that of bulk c-Si. Studies on porous and microcrystalline silicon showed that as the crystallite size decreases, momentum conservation will be relaxed and Raman active modes will not be limited to the center of the Brillouin zone. As surface modes of a finite crystal contribute to the Raman spectrum a downshift of the optical peak frequency is observed [14], [10]. In our experiments, the shift of the F_{2g} Raman peak towards that of bulk silicon and the reduction of its FWHM after annealing, can be explain by an increased crystallinity of silicon. These first experiments show evidently that Raman spectroscopy represents a method to monitor the overall crystallographic state of core-shell nanowires.

In order to characterize Si-Si core-shell nanowires with respect to a potential implementation in electronic devices, SiNWs were electrically integrated by means of conventional microfabrication. Titanium (thickness 5 nm) and aluminum (thickness 300 nm) were evaporated and locally deposited by means of PMMA resist and electron-beam-lithography to act as conductor material for Ohmic contacts. The p-doped core and n-doped shell nanowire shown in Fig. 6(a) exhibit a radial pn-junction as well as an axial pn-junction encoded geometrically by a nanowire kink created during the VLS nanowire core growth. The synthesis of kinked silicon nanowires has been previously illustrated by [15]. The structures show overall the expected semiconducting charge transport properties, such as rectifying characteristics [see Fig. 6(b)] assuring fully usability for nanoscale electronic devices.

B. Ge-Si Core-Shell Nanowires

In addition to Si-Si core-shell homo-junctions, the synthesis of Ge-Si core-shell nanowires provides a tool for hetero-junction device assembly. Reference [1] have shown that by stacking different shell structures onto the nanowire core, higher light absorption efficiencies can be achieved. Besides increased light absorption properties, such core-shell nanowires can be utilized to be used as nanofluidic devices after the removal of the Ge core, which is achieved by H_2O_2 etching resulting in a Si nanotube structure. The application of Si nanotubes with respect to ion-sensitive nanofluidic channels have been shown by [7].

The electrical behavior of Ge-Si core-shell nanowires, before and after core removal is illustrated in Fig. 7. The slight non-linearity around 0 V or the so-called Schottky behavior originates most likely from non-ideal Ohmic contacts.

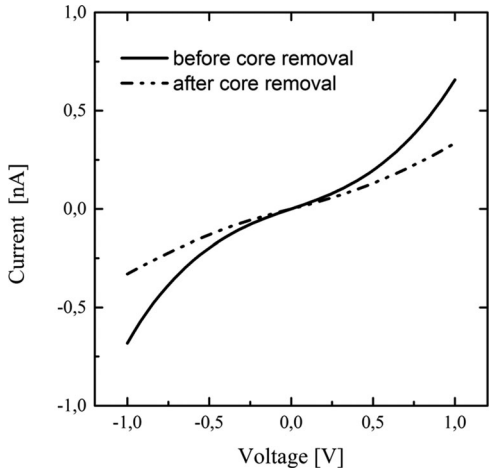

Fig. 7. Current-voltage behavior of Ge-Si Core-shell nanowires before and after removal of the germanium core. The reduced electrical conductivity of the structure after core etching stems mainly from a reduction in the area of the structure.

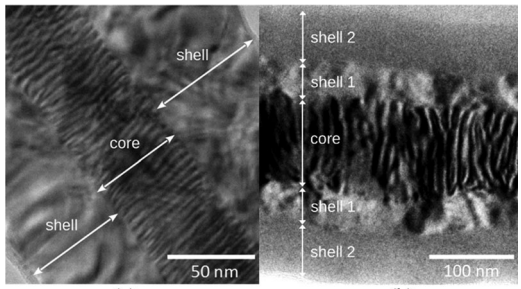

Fig. 8. TEM images of Ge-Si core-shell nanowires. (a) Germanium nanowire core and crystalline silicon shell deposited at 650 °C. The overlapping crystal planes of core and shell structures cause Moiré patterns to appear on the core. (b) Germanium nanowire core and silicon shell with a crystalline structure deposited at 650 °C (labeled as shell 1) followed by a second silicon shell with an amorphous structure deposited at 500 °C (labeled as shell 2) illustrating the possibility of growing silicon shell layers with different microstructure on germanium nanowire core.

Similar to the Si-Si core-shell nanowires, we illustrate the possibility of tuning the crystalline properties also of Ge-Si core-shell nanowires, which can potentially influence electrical transport and light absorption properties.

Two different synthesis conditions that lead to different silicon shell structures are illustrated in the TEM images of Ge-Si core-shell nanowires see [Fig. 8(a) and (b)]. Fig. 8(a) represents a Ge-Si core-shell nanowire, for which the synthesis of the silicon shell was carried out at 650 °C leading mainly to a single-crystalline shell structure by epitaxial Si shell growth onto the single-crystalline Ge core. Fig. 8(b) shows the shells synthesized as-per the double-step protocol. In contrary to the Si-Si core-shell nanowires, the first shell (shell 1) grown at 650 °C appears single-crystalline while the second shell, grown at 500 °C, appears as before amorphous. Although the overall tendencies in crystallographic morphology and behavior of the shell growth of Ge-Si core-shell nanowires are similar to the Si-Si core-shell nanowires, further experiments are required and ongoing.

IV. Conclusion

In summary, this paper presents a detailed study of synthesis methods of Si-Si and Ge-Si core-shell nanowires. Two types of Si-Si core-shell nanowires are characterized using HRTEM and Raman spectroscopy. In addition to Si-Si homo-junctions, synthesis of Ge-Si core-shell hetero-junctions is discussed. It is shown that the results obtained by TEM and Raman spectroscopy are overall coherent and provide details on the nature of as-grown and post-annealed shell structures. The result of this work illustrate that in addition to being able to adjust nanowire length (VLS growth) and diameter (CVD shell growth), the crystallinity of the shell can be adjusted by changing the synthesis conditions and performing adequate post-annealing steps.

Acknowledgment

The authors would like to thank M. Hocker and A. Djaberi with Raman spectroscopy measurements is appreciated.

References

[1] S. Wang, X. Yan, X. Zhang, J. Li, and X. Ren, "Axially connected nanowire core-shell p-n junctions: a composite structure for high-efficiency solar cells," *Nanoscale Res. Lett.*, vol. 10, no. 1, pp. 0–6, 2015.
[2] L. J. Lauhon, M. S. Gudiksen, D. Wang, and C. M. Lieber, "Epitaxial core-shell and core-multishell nanowire heterostructures.," *Nature*, vol. 420, no. 6911, pp. 57–61, 2002.
[3] Y. Dong, G. Yu, M. C. Mcalpine, W. Lu, and C. M. Lieber, "Si /a-si core/shell nanowires as nonvolatile crossbar switches," *Nano Lett.*, vol. 8, no. 2, pp. 386–391, 2008.
[4] C. K. Chan *et al.*, "High-performance lithium battery anodes using silicon nanowires," *Nat. Nanotechnol.*, vol. 3, pp. 31–35, 2008.
[5] C. Shell, S. Nanowires, M. M. Adachi, M. P. Anantram, and K. S. Karim, "Optical properties of crystalline - amorphous core−shell silicon nanowires," *Nano Lett.*, vol. 10, no. 10, pp. 4093–4098, 2010.
[6] W. Lu, J. Xiang, B. P. Timko, Y. Wu, and C. M. Lieber, "One-dimensional hole gas in germanium silicon nanowire heterostructures," *Proc. Natl. Acad. Sci. U. S. A.*, vol. 102, no. 29, pp. 10046–10051, 2005.
[7] N. Hibst, A. M. Steinbach, and S. Strehle, "Fluidic and electronic transport in silicon nanotube biosensors," in *MRS Advances*, 2016.
[8] W. Lu, J. Xiang, B. P. Timko, Y. Wu, and C. M. Lieber, "One-dimensional Hole gas in germanium/silicon nanowire heterostructures," *Proc. Nat. Acad. Sci. U. S. A.*, vol. 102, no. 29, pp. 10046–10051, 2005.
[9] H. J. Fan, P. Werner, and M. Zacharias, "Semiconductor Nanowires: From Self-Organization to Patterned Growth," *Reviews*, vol. 2, no. 6, pp. 700–717, 2006.
[10] S. Veprek, Z. Iqbal, Z. Iqbal, S. Veprek, S. Veprek, and Z. Iqbal, "Raman scattering from hydrogenated microcrystalline and amorphous silicon," *J. Phys. c.*, vol. 15, no. 2, pp. 377–392, 1982.
[11] D. P. Yu *et al.*, "Nanoscale silicon wires synthesized using simple physical evaporation," *Appl. Phys. Lett.*, vol. 3458, no. 1998, pp. 21–24, 2016.
[12] R. Wang *et al.*, "Raman spectral study of silicon nanowires: High-order scattering and phonon confinement effects," *Phys. Rev. B*, vol. 61, no. 24, pp. 827–832, 2000.
[13] J. Qi, J. M. White, A. M. Belcher, and Y. Masumoto, "Optical spectroscopy of silicon nanowires," *Chem. Phys. Lett.*, vol. 372, pp. 763–766, 2003.
[14] B. Li, D. Yu, and S. Zhang, "Raman spectral study of silicon nanowires," vol. 59, no. 3, pp. 1645–1648, 1999.
[15] B. Tian, P. Xie, T. J. Kempa, D. C. Bell, and C. M. Lieber, "Single-crystalline kinked semiconductor nanowire superstructures," *Nat. Nanotechnol.*, vol. 4, no. 12, pp. 824–829, 2009.

Authors' photographs and biographies not available at the time of publication.